Deformation behavior of a 2219 Al alloy

R. Kaibyshev [a], O. Sitdikov [a,*], I. Mazurina [a], D.R. Lesuer [b]

[a] *Laboratory of Plastic Deformation of Solid State, Institute for Metals Superplasticity Problems RAS, Khalturina 39, Ufa 450001, Russia*
[b] *Lawrence Livermore National Laboratory, L-342 PO Box 808, Livermore, CA 94551, USA*

Abstract

The deformation behavior of a 2219 aluminum alloy was studied in the temperature range from 250 to 500 °C. The results, which cover four orders of magnitude in strain rate, show an increasing apparent stress exponent and an increasing apparent activation energy with decreasing temperature. It is shown that the 2219 aluminum alloy exhibits threshold behavior, like aluminum alloys produced via powder metallurgy technique. The introduction of a threshold stress into the analysis leads to stress exponent of ~ 7 and a true activation energy of about 90 kJ mol^{-1} in the temperature range 250–450 °C. At $T = 500$ °C, the true stress exponent, n, is equal to 5 and true activation energy is equal to 143 kJ mol^{-1}. The normalized threshold stress exhibits a strong temperature dependence. The value of the energy term, Q_o, is about 35 kJ mol^{-1} in the temperature range 250–450 °C and tends to decrease at higher temperature. The operating deformation mechanism is discussed in terms of the transition from low temperature climb to high temperature climb with increasing temperature.

Keywords: Plastic deformation; Creep; Threshold stress; 2219 Al alloy

1. Introduction

The deformation behavior of Al–Cu alloys has been extensively studied in two different temperature intervals [1–5]. The first temperature interval is the low temperature range from 100 to 250 °C where copper precipitates provide strengthening due to the interaction between precipitates and dislocations [1–3]. Work in this low temperature interval was motivated by the importance of creep properties of Al–Cu alloys under service conditions. The second temperature interval is the range of pre-melting temperatures (500–580 °C) where copper exists in solid solution [4,5]. In this temperature interval, Mohamed et al. [4,5] reported on a viscous dislocation glide phenomenon. In the intermediate temperature range from 250 to 500 °C, the creep behavior of an Al–Cu alloy has not been examined yet in detail.

The present study was carried out to provide detailed information on the deformation behavior of a 2219 aluminum alloy at these intermediate temperatures. This temperature range is widely used for working the

2219 aluminum alloy. An examination of deformation mechanisms operating in this interval is important for discussing the physical basis for plastic deformation and development of new routes of thermomechanical processing of Al–Cu alloys. In addition, it can be expected that the 2219 alloy containing Al_3Cr and Al_3Zr dispersoids may exhibit threshold behavior. It is well known that aluminum alloys produced by powder metallurgy techniques exhibit threshold behavior due to the presence of nanoscale alumina particles [6–8]. At the same time, other authors [9] have shown that an Al–5%Cr–2%Zr alloy produced by rapid solidification exhibited threshold behavior. At present, experimental evidence in support of this expectation is not available.

2. Materials and experimental technique

The 2219 aluminum alloy with the chemical composition Al–6.4%Cu–0.3%Mn–0.18%Cr–0.19%Zr–0.06%Fe was manufactured at the Kaiser Aluminum Center for Technology by direct chill casting. The alloy was then homogenized at 530 °C for 6 h and cooled slowly in a furnace to provide an equilibrium two phase structure. The alloy had an initial grain size of about

* Corresponding author. Tel./fax: +7-3472-253-856.
E-mail address: sitdikov@imsp.da.ru (O. Sitdikov).

120 μm. Compression specimens 9 mm in diameter and 11 mm high were machined from the alloy ingot. The samples were deformed in compression at constant crosshead speed using a Scheck RMS-100 testing machine. Tests were carried out over the temperature range 250–500 °C in 50 °C increments at an initial strain rate in the range from 1.5×10^{-6} s^{-1} up to 3×10^{-2} s^{-1} At an initial strain rate of 3×10^{-4} s^{-1}, tests were performed every 25 °C.

For surface examination, specimens were mechanically polished and covered by boric acid to prevent oxidation. The specimens were then strained to $\varepsilon = 0.16$ at strain rates of 3×10^{-4} and 3×10^{-2} s^{-1} at 250 and 500 °C. A SEM JSM-840 was used to observe the surface features. Samples were also examined in a transmission electron microscope (TEM). For these examinations, samples were cut from the gauge section of deformed specimens and thinned to about 0.25 mm. Discs with 3 mm diameter were cut and electropolished to perforation with a Tenupol-3 twinjet polishing unit using a 20% nitric acid solution in methanol at −38 °C and 20 V. The thin foils were examined using a JEOL-2000EX TEM with a double-tilt stage at an accelerating potential of 160 kV. The lattice dislocation density was determined by the number of dislocation intersections with the foil surface, as well as by a line-intercept method [10].

3. Results

3.1. The shape of σ–ε curves

Typical true stress–true strain curves in the temperature range 250–500 °C at a fixed strain rate of 3×10^{-4} s^{-1} (Fig. 1a) and at fixed temperatures of 250, 400 and 500 °C and two different initial strain rates

$(7.5 \times 10^{-5}$ and 3×10^{-2} s^{-1}) (Fig. 1b) are presented in Fig. 1. Almost all curves exhibit a well-defined steady state. Minor strain hardening during plastic deformation takes place at $T = 250$ °C and $\dot{\varepsilon} = 3 \times 10^{-4}$ s^{-1}.

3.2. The variation of steady-state stress with strain rate

Fig. 2a shows the variation of strain rate with flow stress plotted on logarithmic axes. The experimental data in the plot can be represented accurately by straight lines. The results demonstrate that a power-law equation [11] appears valid from 250 to 500 °C:

$$\dot{\varepsilon} = A\left(\frac{\sigma}{G}\right)^{n} \exp\left(\frac{-Q}{RT}\right), \tag{1}$$

where $\dot{\varepsilon}$ is the strain rate, A is a constant, n is the stress exponent, σ is steady state flow stress, G is the shear modulus, Q is the activation energy for plastic deformation, R is the gas constant and T is the absolute temperature. The slope of the lines provides the stress exponent n. The values of n are indicated on the figure. The stress exponent decreases from n $\sim$ 16 at the lowest temperature of 250 °C to n $\sim$ 6.8 at the highest temperature of 500 °C. In the temperature range 250–350 °C, the values of the stress exponent vary from 9 to 16 and are higher than the highest value of the stress exponent n of 8 typically reported for the power law behaviour [1,12,13]. These high stress exponents suggest that the deformation behavior of the 2219 aluminum alloy can be described in terms of the exponential relation [11,14]:

$$\dot{\varepsilon} = B\exp(\beta\sigma)\exp\left(\frac{-Q}{RT}\right), \tag{2}$$

where B is a constant and β is a coefficient. In order to check the validity of Eq. (2), the results were analyzed on a semi-logarithmic plot as shown in Fig. 2b. No satisfactory linear fit is observed even in the tempera-
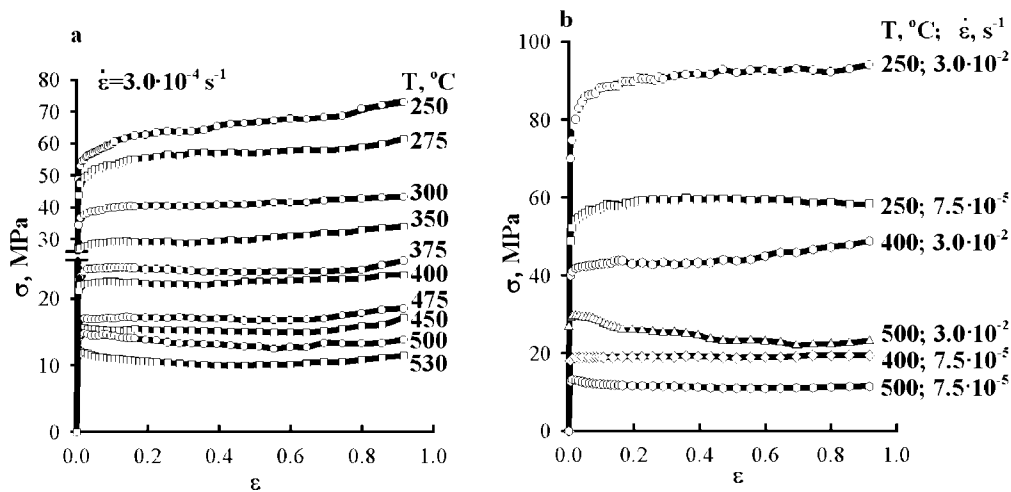

Fig. 1. True stress–true strain curves for the 2219 Al alloy tested: (a) at an initial strain rate of 3×10^{-4} s^{-1} in the temperature range 250–530 °C; (b) at two different initial strain rates, 7.5×10^{-5} and 3×10^{-2} s^{-1} and 250–500 °C.
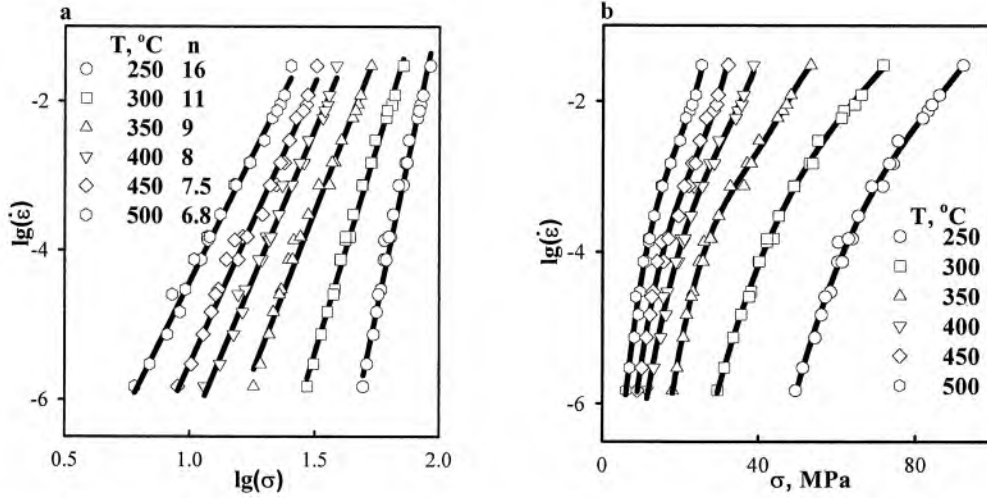
Fig. 2. Plot of strain rate versus steady state flow stress on (a) logarithmic scale; (b) semi-logarithmic scale.
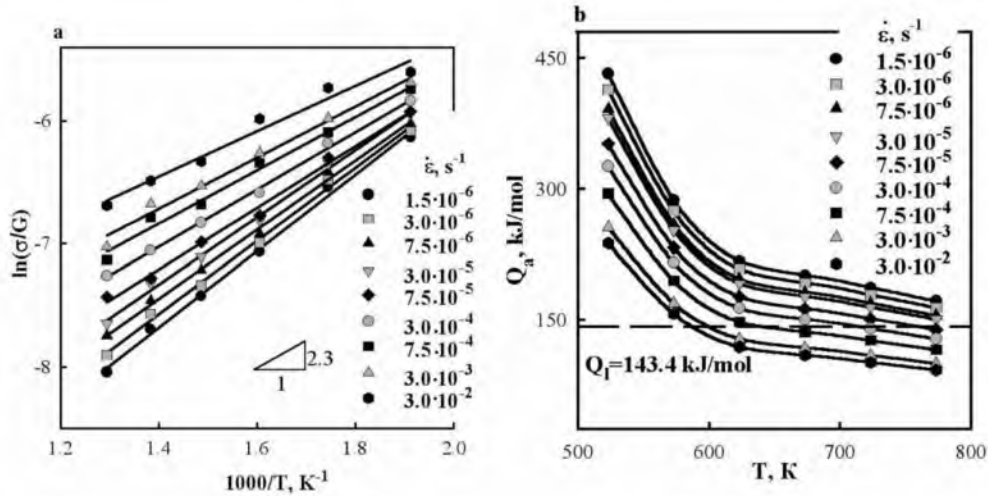

Fig. 3. (a) Shear modulus compensated applied stress versus inverse absolute temperature; (b) temperature dependence of the apparent activation energy, Q_a.

ture range 250–350 °C, where the regression coefficient r was found to be lower ($r = 0.95$) relative to the logarithmic plot where the value of r is equal to 0.99. Thus, a power-law relationship is appropriate at all temperatures and strain rates examined. This result is unusual because it is well known [14] that the data can be equally well described by Eq. (1) and Eq. (2) when $n \geq 8$ and $\beta \leq 0.065$ MPa^{-1}.

3.3. The activation energy for plastic deformation

The apparent activation energy for plastic deformation, Q_a, was determined using the procedure described by Pickens et al. [15]. Eq. (1) can be converted to:

$$\ln\left(\frac{\sigma}{G}\right) = \ln\left(\frac{\dot{\varepsilon}}{A}\right)^{1/n} + \frac{Q_a}{Rn} \times \frac{1}{T} \qquad (3)$$

The values of Q_a were obtained graphically by logarithmically plotting the normalized stress, σ/G, against the inverse of the absolute temperature and taking the slope of the data to be Q_a/Rn (Fig. 3a) for different values of the initial strain rate. In the calculations, the shear modulus for pure Al was used which can be defined as a function of temperature as [8]:

$$G = (3.022 \times 10^4) - 16T, \text{ MPa} \qquad (4)$$

The dependence of $\ln(\sigma/G)$ on $1/T$ is linear at all temperatures examined. The slope of these lines tends to decrease with increasing strain rate. As a result, there is a strain rate dependence of the apparent activation energy values (Fig. 3b). The temperature dependence of the apparent activation energy obtained is unusual and in contrast to the reported temperature dependence of the activation energy for pure Al [16], as well as for other metallic materials [11,17]. For $\dot{\varepsilon} = 3 \times 10^{-4}$ s^{-1},
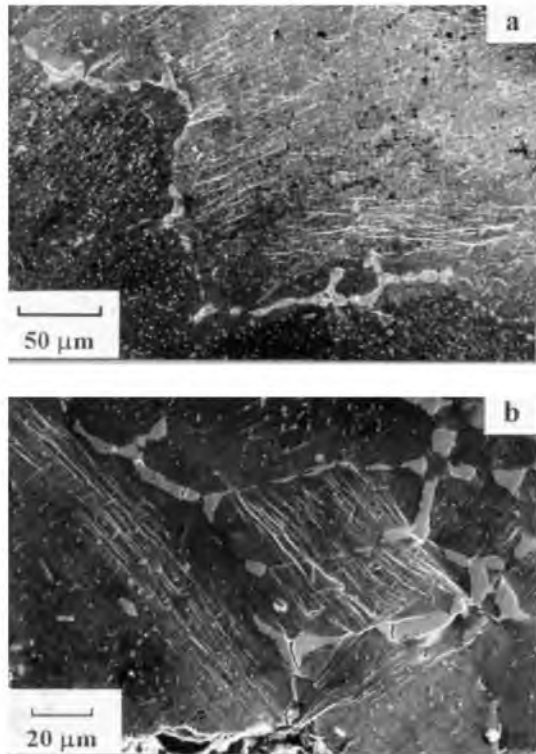
Fig. 4. Surface observations of the 2219 Al alloy samples strained up to $\varepsilon = 0.16$ at $T = 250$ °C: (a) $\dot{\varepsilon} = 10^{-4}$ s^{-1}; (b) $\dot{\varepsilon} = 10^{-2}$ s^{-1}.
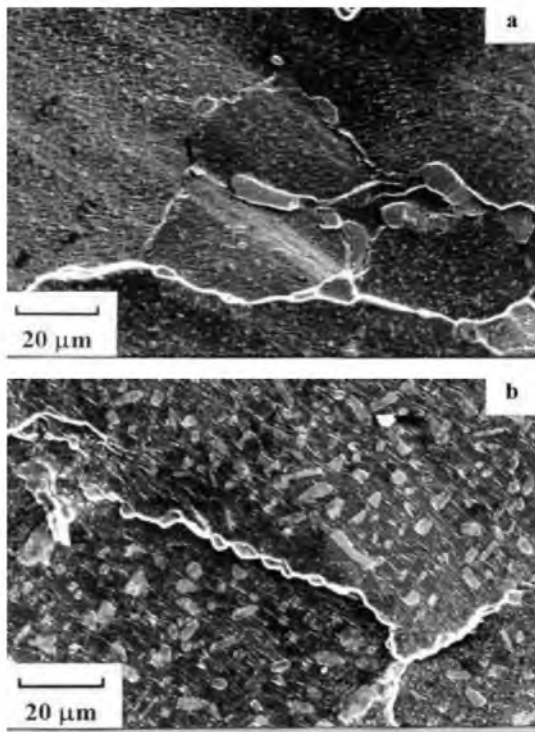

Fig. 5. Surface observations of 2219 Al alloy strained up to $\varepsilon = 0.16$ at $T = 500$ °C: (a) $\dot{\varepsilon} = 10^{-4}$ s^{-1}; (b) $\dot{\varepsilon} = 10^{-2}$ s^{-1}.

the values of Q_a sharply decrease from ~ 326 kJ mol^{-1} at $T = 250$ °C to ~ 151 kJ mol^{-1} at $T = 400$ °C. With further temperature increase to 500 °C, the values of Q_a tend to decrease to the value of activation energy for lattice diffusion in pure aluminum ($Q_l = 143.4$ kJ mol^{-1} [18]). Thus, there is a well-defined decrease in Q_a with increasing temperatures.

3.4. Surface observations

Surface observations showed that temperature and strain rate did not have a significant effect on dislocation glide (Figs. 4 and 5). At $T = 250$ °C and $\dot{\varepsilon} = 10^{-4}$ s^{-1}, two families of long slip features were observed (Fig. 4a). This is evidence for dislocation slip on multiple system. Steps on slip lines and the wavy shape of slip features are indicative of weak cross-slip. Dislocation glide is essentially uniform. An increase in strain rate up to 10^{-2} s^{-1} results in intense localization of dislocation glide on the microscale level (Fig. 4b). The slip lines form bands of localized deformation.

Uniform deformation takes place at $T = 500$ °C (Fig. 5a and b). Short and wavy slip lines, which were observed both near the initial boundaries and inside the grains, are indicative of extensive cross-slip. Single dislocation slip highly dominates. Thus, an increase in temperature and a decrease in strain rate yield increased uniformity of dislocation glide and result in a transition from multiple to single slip. Cross-slip is facilitated by increasing temperature. Particles of secondary phases play the role of barriers to the propagation of slip lines. Surface observations suggest that secondary phases can be responsible for initiating extensive cross slip, which permits bypassing of the particles by mobile dislocations.

3.5. Microstructure observation

Second-phase particles (Fig. 6a) were identified by TEM analysis as Al$_3$Cr and Al$_3$Zr with average sizes 0.1 μm and 20 nm, respectively, in the initial state. It is known that the Al$_3$Zr particle boundaries can be both coherent as well incoherent [19]. Coherent boundaries exhibit coherent stress fields, which are distinguished by TEM as non-uniform diffraction contrast near a dispersoid. It was observed that at least 85% of the Al$_3$Cr and Al$_3$Zr dispersoids exhibited incoherent boundaries. No subgrain structure was observed in the starting material.

The microstructure developed during deformation to a moderate strain of 0.36 may be divided into two categories. At $T < 450$ °C, a poor-defined cell structure is formed (Fig. 6b). Separate cell boundaries consisting of tangled dislocations are often observed and dislocation cells are rarely observed. The formation of a subgrain structure was detected in the samples deformed at $T \geq 450$ °C (Fig. 6c). Selected area diffrac-
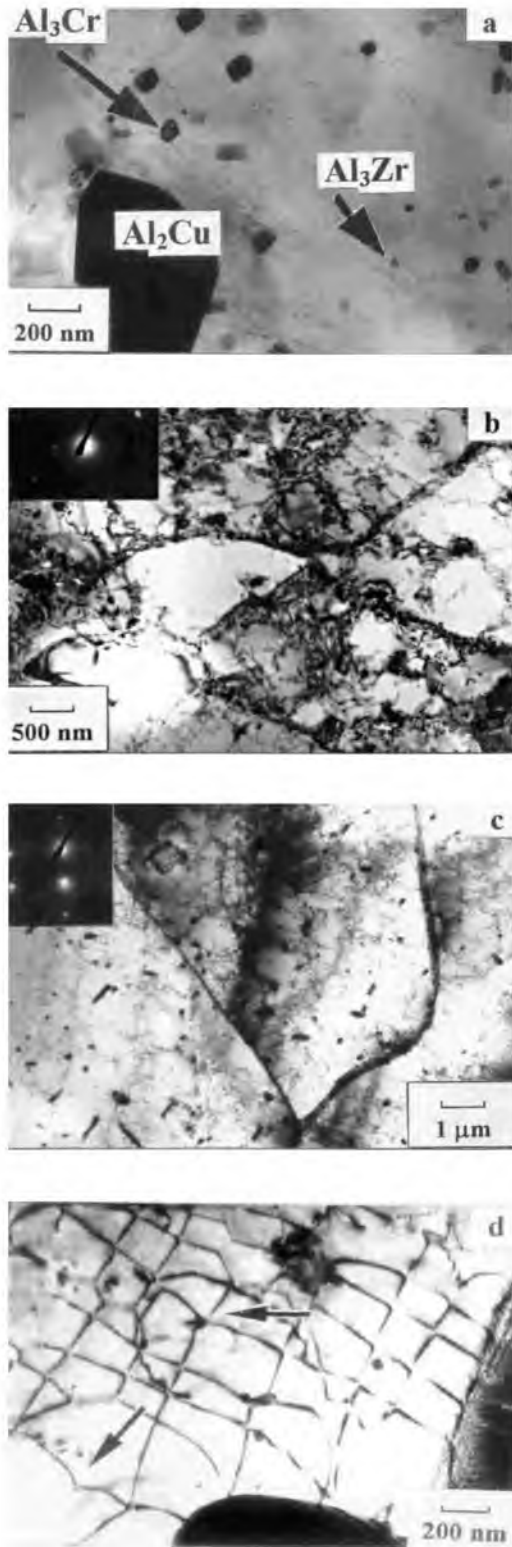
Fig. 6. TEM image of 2219 Al alloy; (a) initial state; (b) sample strained to $\varepsilon = 0.36$ at $\dot{\varepsilon} = 3 \times 10^{-4}$ s^{-1} and $T = 300$ °C; (c) sample strained to $\varepsilon = 0.36$ at $\dot{\varepsilon} = 3 \times 10^{-4}$ s^{-1} and $T = 475$ °C; (d) sample strained to $\varepsilon = 0.36$ at $\dot{\varepsilon} = 10^{-2}$ s^{-1} and $T = 400$ °C (arrows indicate detachment of dislocations from dispersoids).

tion patterns taken from both structures show that the misorientation of deformation induced boundaries is small ($< 2°$) (Fig. 6b and c). Thus, plastic deformation results in the formation of dislocation boundaries with low misorientation.

Fig. 7 represents the dependence between density of separate lattice dislocations, ρ, and the modulus-normalized applied stress, σ/G. The classic dependence [11]:

$$\rho = \left(\frac{\sigma}{G}\right)^{1/2} \tag{5}$$

holds for the present 2219 alloy. The dislocation density tends to decrease from $\sim 10^{14}$ to $\sim 10^{13}$ m^{-2} with increasing temperature from 250 to 475 °C.

An attractive interaction between mobile dislocations and dispersoids was found (Fig. 6d). Lattice dislocations overcome dispersoids and detach from them. A curvature of detaching dislocation is an evidence for the attractive particle-dispersoid interaction. It can be seen (Fig. 6d) that the process of detachment is facilitated by local stress caused by dislocation tension.

4. Discussion

An inspection of the deformation behavior of the 2219 aluminum alloy and data of TEM observations suggest that this material could exhibit threshold behavior. This possibility follows from Fig. 2a where in the temperature range 250–350 °C, a minor increment in the stress exponent, n, with decreasing strain rate can be observed. Such a stress dependence of strain rate is consistent with an existence of a threshold stress [20]. This conclusion is supported by unrealistically high values of the apparent activation energy in the low temperature range where high values of the stress exponent are observed. In addition, the direct observations of detachment of lattice dislocations from dispersoids unambiguously testify to the existence of threshold
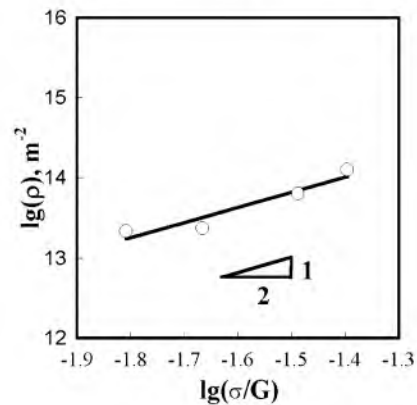

Fig. 7. Plot of lattice dislocation density, ρ, against the modulus-normalized applied stress, σ/G, for the 2219 Al alloy at $\dot{\varepsilon} = 10^{-2}$ s^{-1}.
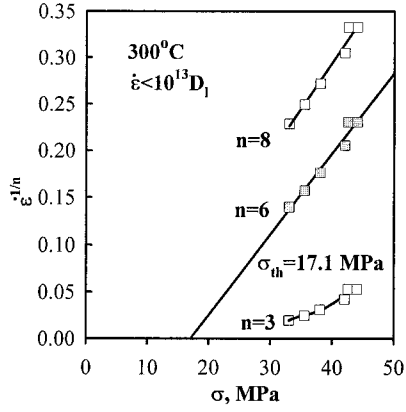
Fig. 8. Plot of $\dot\varepsilon^{1/n}$ against σ for the 2219 Al alloy at $T = 300$ °C.

Table 1
Threshold stress at different temperatures

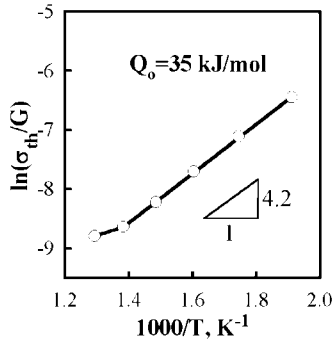| T (°C)	250	300	350	400	450	500
n	6	6	6	6	6	5
σ_{th} (MPa)	34.6	17.1	9.2	5.2	3.3	2.7

Fig. 9. Plot of the logarithmic of the normalized threshold stress versus reciprocal absolute temperature.

stress [21,22]. Thus, it can be assumed that the deformation behavior of the 2219 Al alloy cannot be described by a single expression of the form given by Eq. (1) but is described more realistically by an equation accounting for the threshold stress [6–8,20]:

$$\dot\varepsilon = A\left(\frac{\sigma - \sigma_{th}}{G}\right)^n \exp\left(\frac{-Q_c}{RT}\right), \tag{6}$$

where σ_{th} is threshold stress, $\sigma - \sigma_{th}$ is an effective stress driving the deformation observed and Q_c is a 'true' activation energy for plastic deformation.

4.1. Estimation of threshold stresses

A standard procedure was used to determine the threshold stress [6–8,20]. The experimental data at a single temperature were plotted as $\dot\varepsilon^{1/n}$ against the steady state flow stress σ on a double-linear scale for all

temperatures examined. Notably, for the two temperatures 250 and 300 °C, the high-strain rate data points lying above the Sherby–Burke criterion [23]:

$$\frac{\dot\varepsilon}{D_1} = 10^{13}, \text{ m}^{-2} \tag{7}$$

where D_1 is the lattice self-diffusion coefficient calculated as [8]:

$$D_1 = 1.86 \times 10^{-4}\exp\left(\frac{-143.4 \times 10^3}{RT}\right), \text{ m}^2 \text{ s}^{-1} \tag{8}$$

were discarded and only data lying below this theoretical limit were included in the analysis. These data in the strain rate interval were best fitted to a straight line by varying the n values. The n value exhibiting the highest regression coefficient in a linear fit was taken as the true stress exponent value. The intercept on the stress axis yields the σ_{th} value, which, in principle, is independent of the applied stress. Fig. 8 shows a typical plot $\dot\varepsilon^{1/n}$ versus σ at $T = 300$ °C for $n = 3$, 6, 8, respectively. Inspection of Fig. 8 indicates that the stress exponent of 6 yields the best linear fit between $\dot\varepsilon^{1/n}$ and σ for $n = 3$ and 8, the data of the plots exhibit clear concavity and convexity, respectively.

Values of threshold stress obtained and the true stress exponent, n, are summarized in Table 1 as a function of testing temperature. Inspection of Table 1 shows that a stress exponent of 6 yields the best linear fit between $\dot\varepsilon^{1/n}$ and σ in the temperature range 250–450 °C. At $T = 500$ °C, the stress exponent $n = 5$ is the true stress exponent. The values of threshold stress can be as much as 75% of the value of the applied stress at $T = 250$ °C and the lowest strain rate examined and tends to decrease with increasing temperature to 10% at $T = 500$ °C. Notably, the values of threshold stress obtained are at least two times lower than that reported in [1] for an Al–6%Cu–0.6% Mg alloy additionally alloyed with 1.8%Mn, 0.1%Cr, 0.4%Ag, 0.4%Zr, 0.2%V and 0.25%Ti at $T = 250$ °C and lower in comparison with data for an Al–5%Cr–2%Zr alloy by factors of 1.5–4 at similar temperatures [9]. The threshold stresses obtained are essentially similar to those reported for the 2124, 6061 and 2024 aluminum alloys produced by powder metallurgy techniques [6,7,20] in the temperature interval 350–400 °C.

Fig. 9 shows the temperature dependence of the modulus-normalized threshold stress. The data follow the equation [7,8,20]:

$$\frac{\sigma_{th}}{G} = B_o\exp\left(\frac{Q_o}{RT}\right), \tag{9}$$

where B_o is a constant and Q_o is an energy term representing the activation energy for a dislocation to overcome an obstacle. The value of Q_o calculated from the slope of the plot in the temperature range 250–450 °C in Fig. 9 is 35 kJ mol^{-1}. This value is slightly

higher than the energy reported for 2124 (27.5 kJ mol^{-1}) [20], 6061 (19.3 kJ mol^{-1}) [6] and 2024 (23 kJ mol^{-1}) [7] aluminum alloys produced via powder metallurgy techniques. Although there is only one data point above 450 °C, Q_o seems to decrease with increasing temperature.

4.2. Activation energy

To determine the activation energy for deformation, the normalized effective stresses $((\sigma - \sigma_{th})/G)$ are plotted as a function of $1/T$ on a semi-logarithmic scale at a fixed strain rate (Fig. 10a) [15]. The data can be divided into two temperature intervals (250–450 and 450–500 °C) that are distinguished by the slope k. In these temperature intervals, k is ~ 1.9 and ~ 3.4, respectively. The slope in Fig. 10a shows a very small strain rate dependence, which supports the validity of the threshold stress values determined.

Values of true activation energy (Q_c) for plastic deformation were computed assuming that Eq. (6) adequately describes the deformation behavior of the 2219 Al alloy. Results are shown in Fig. 10b. It is seen that depending on strain rate, $Q_c = 90 \pm 7$ kJ mol^{-1} was measured in the temperature range $T = 250$–450 °C. The average value of Q_c is close to that for pipe diffusion in Al (82 kJ mol^{-1}) [18]. At $T = 500$ °C, $Q_c = 143 \pm 15$ kJ mol^{-1} is similar to the activation energy for self-diffusion in Al (143.4 kJ mol^{-1}) [18]. Thus, the incorporation of a threshold stress in the activation energy analysis provides realistic values for the true activation energy at $T < 400$ °C.

4.3. An examination of normalized deformation data

Fig. 11a shows a double logarithmic plot of the normalized strain rate, $\dot{\varepsilon}kT/D_{eff}Gb$, versus the normalized effective stress, $(\sigma - \sigma_{th})/G$ for the 2219 aluminum alloy. The Burgers vector was taken as $b = 2.86 \times 10^{-10}$ m and an effective diffusion coefficient [13,24,25] was used:

$$D_{eff} = f_1 D_1 + f_{pd} D_{pd}, \tag{10}$$

where D_1 and D_{pd} are the lattice self-diffusion and pipe-diffusion coefficients, and f_1 and f_{pd} are the fractions of atoms participating in lattice and pipe diffusion, respectively. The lattice diffusion coefficient was taken from Eq. (8). The value of f_1 was assumed to be 1. The term associated with the contribution of pipe-diffusion to the total diffusion process was determined for pure Al according to data presented in [24] as:

$$f_{pd} D_{pd} = 10 \left(\frac{a_c}{b^2} \right) \times \left(\frac{\sigma}{G} \right)^2 D_{pd}, \tag{11}$$

$$a_c D_{pd} = 7.0 \times 10^{-25} \exp \left(\frac{-82 \times 10^3}{RT} \right), \ m^4 s^{-1} \tag{12}$$

where a_c is the area of cross-section of the dislocation core.

It is seen from Fig. 11a, that there are two different intervals for plastic deformation of the 2219 Al alloy. At $\dot{\varepsilon}kT/(D_{eff}Gb) < 10^{-11}$, there is a well-defined power-law relationship with a stress exponent, $n = 5$. Analysis by previous authors [11–13,16] has shown that if n is in the range from 3 to 5 and Q_c is equal to Q_1, then the most probable rate-controlling mechanism for creep is the climb of edge dislocations. In this case, the creep
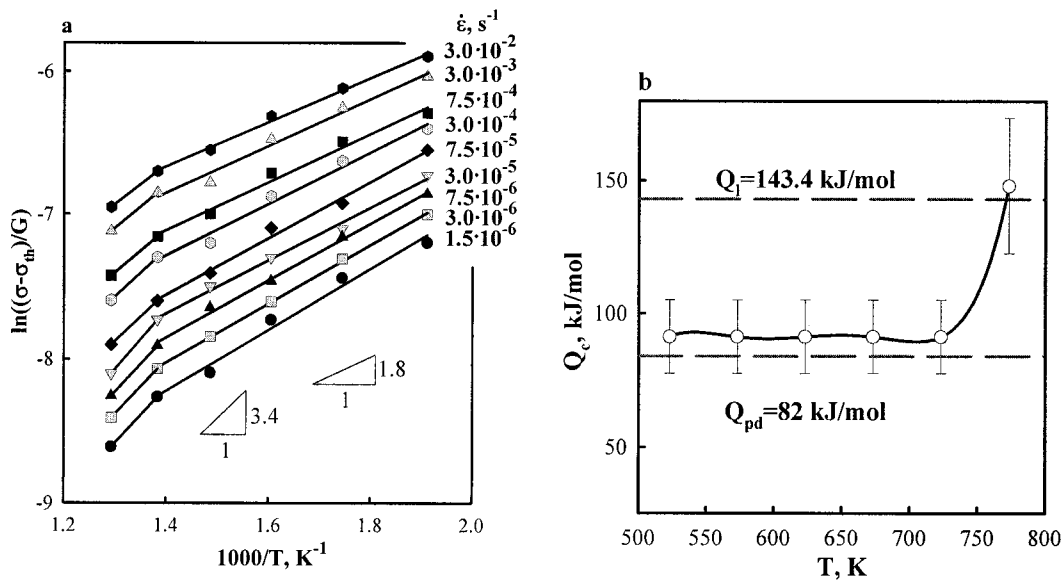

Fig. 10. (a) Shear modulus compensated effective stress versus inverse absolute temperature; (b) temperature dependence of the true activation energy, Q_c.
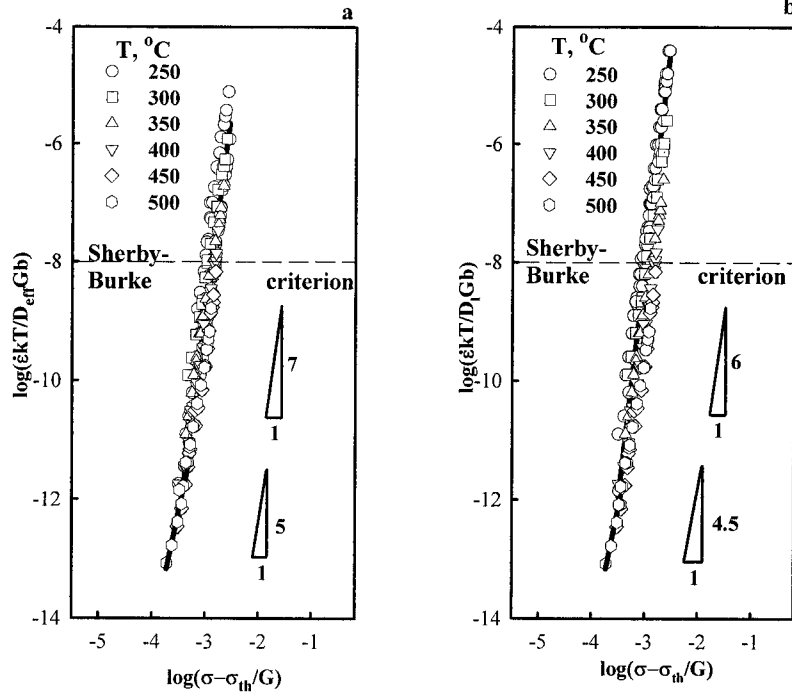
Fig. 11. Normalized strain rate versus normalized stress for the 2219 aluminum alloy. (a) Effective diffusion coefficient, D_{eff}, was used for strain rate normalization; (b) lattice diffusion coefficient, D_l was used for strain rate normalization.

deformation is controlled by lattice diffusion. Therefore, based on the relative agreement of the measured and anticipated values of n and Q_c, a high-temperature dislocation climb mechanism can be expected to control the creep behavior of Al 2219 alloy at $\dot{\varepsilon}kT/(D_{eff}Gb) < 10^{-11}$. This temperature/strain rate range is a region for true hot deformation of the 2219 aluminum alloy (typically observed at $T \geq 475$ °C) where extensive dislocation rearrangements by climb take place. As a result, the formation of a subgrain structure after small strain and high uniformity of dislocation glide are observed in this temperature range. For values of $\dot{\varepsilon}kT/(D_{eff}Gb)$ above 10^{-11}, the slope of the straight line on the $\dot{\varepsilon}kT/(D_{eff}Gb)$ versus $(\sigma - \sigma_{th})/G$ plot is equal to 7.

An inspection of the normalized deformation data shows that a classic transition from high temperature climb (controlled by vacancy diffusion through the lattice) to low temperature climb (controlled by vacancy diffusion along dislocation cores) takes place. This transition results in an increase in the stress exponent from $n = 5$ to 7 in accordance with the rule $n = n + 2$ [11–13,16,17]. Concurrently, a decrease in true activation energy for plastic deformation from $Q_c = Q_l$ to $Q_c = Q_{pd}$ takes place. This change is clearly indicative of the transition from high temperature climb, controlled by lattice diffusion to low temperature climb with decreasing temperature [11,17,25]. This transition results in a significant decrease in the rate of dislocation climb and restricts the ability of lattice dislocations to rearrange. As a result, no well-defined

low angle boundaries are formed after a true strain of 0.36. In addition, a localization of dislocation glide occurs in spite of the fact that the cross-slip plays an important role in dislocation rearrangement in all temperature ranges examined. Therefore, this transition can be considered as the incipient point for progressive transition from hot deformation to warm deformation. Notably, the upper bound for the region of low temperature climb is defined by the Sherby–Burke criterion $[\dot{\varepsilon}kT/(DGb) \approx 10^{-8}]$, which according to [23] is a criterion for the breakdown of the power law. However, no breakdown is observed at this value of the normalized strain rate in the 2219 alloy.

For comparison, a plot of the normalized strain rate, $\dot{\varepsilon}kT/D_lGb$, against the normalized effective stress, $(\sigma - \sigma_{th})/G$, is depicted in Fig. 11b, which shows that the use of the lattice diffusion coefficient, D_l, for strain rate normalization results in a decrease in values of the stress exponent, n. Data obtained for $T = 500$ and 475 °C can be fitted with high accuracy by a straight line with a slope of 4.5. The data points for lower temperatures can be approximated by a straight line with slope close to 6. In addition, the point of transition from $n = 4.5$ to 6 is located at a higher normalized strain rate than in Fig. 11a. This may be due to the fact that the low temperature dislocation climb plays an important role in plastic deformation of the 2219 alloy even at high temperatures.

The transition from hot deformation to warm deformation in the 2219 Al initiates at a normalized effective

stress of $(\sigma - \sigma_{th})/G \cong 6 \times 10^{-4}$. As shown in Fig. 12, this transition takes place at a similar value of normalized stress in pure aluminum (Fig. 12 is replotted Fig. 7a from [16]). Thus, the range of hot deformation in the 2219 alloy is observed at temperatures more than 200 °C higher than that for pure aluminum [16] due to increased flow stress; such a temperature increase is needed to enhance the rate of dislocation rearrangement by climb or cross-slip. As a result, a gradual decrease in the lattice dislocation density with increasing temperature is caused by an increasing rate of dislocation rearrangements leading to mutual annihilation of dislocations.

4.4. Origin of the threshold stress

The origin of the threshold stress in the 2219 Al alloy is attributed to the incoherent Al_3Cr and Al_3Zr particles which attractively interact with mobile dislocations. These particles play a similar role in plastic deformation as nanoscale oxides in dispersion strengthened
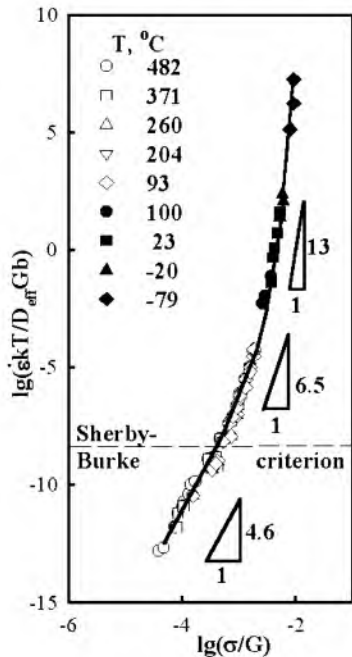
Fig. 12. Normalized strain rate versus normalized stress for Al from data points taken from [16].
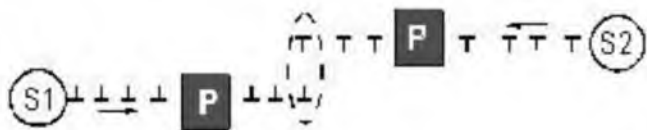
Fig. 13. Schematic diagram of a deformation mechanism consisting of two sequential processes—interaction of a dislocation with a dispersoid and dislocation annihilation by the classic Weertman model [11,30]: S1 and S2 are the dislocation sources; P are the particles of secondary phases.

aluminum alloys [6–8,26–28]. It can be seen from TEM observation that detachment of lattice dislocations from the particles results in the threshold stress. Notably, the existing models for detachment [21,22,29] do not predict a temperature dependence of threshold stress which was observed in the present work.

Thus, the incoherent particles containing transition elements in the 2219 alloy act as barriers to dislocation glide. Fig. 13 schematically represents a modification of the well-known Weertman model [11,30]. A dislocation glides on a crystallographic plane, encounters an incoherent particle, overcomes the dispersoid by climb and detaches from this particle. Further dislocation glide results in the formation of a dislocation dipole consisting of two dislocations of opposite signs. Climb of these dislocations toward one another leads to their annihilation. Therefore, the deformation behavior of the 2219 alloy is controlled by two sequential processes as follows: (1) interaction between a dislocation and an obstacle and (2) dislocation climb. The first process determines the threshold behavior, and the second one controls the general deformation behavior.

5. Conclusions

The deformation behavior of the 2219 aluminum alloy was investigated at temperatures from 250 to 500 °C in the strain rate range from 1.5×10^{-6} up to 3×10^{-2} s^{-1}. Analysis of experimental data of the 2219 Al alloy revealed the presence of a threshold stress at the temperatures examined. The threshold stress was found to be temperature dependent with the energy term, Q_o, of 35 kJ mol^{-1} in the temperature range 250–450 °C.

An incorporation of threshold stresses into the analysis of the deformation behavior reveals two intervals of plastic deformation—a warm deformation range with a true stress exponent of 7 and a hot deformation range with an n of 5. The transition between these two regions takes place at a temperature of about 450 °C and at a normalized effective stress $(\sigma - \sigma_{th})/G \cong 6 \times 10^{-4}$. Notably, the range of hot deformation in the 2219 aluminum is observed at temperatures 200 °C higher than that for pure aluminum.

The true activation energies for plastic deformation, Q_c, were found to be about 90 ± 7 and 143 ± 15 kJ mol^{-1} in the temperature intervals 250–450 °C and at 500 °C, respectively.

Decreasing temperature and increasing strain rate results in localization of dislocation glide. Increasing temperature makes possible cross-slip and a transition from multiple slip to single slip occurs.

At $T > 450$ °C, low angle boundaries are formed after a strain of $\varepsilon = 0.36$ and at $T < 450$ °C, the formation of cell boundaries was found.

Incoherent nanoscale dispersoids in the 2219 Al alloy attractively interact with mobile dislocations. An extensive detachment of lattice dislocation from the particles takes place during deformation. This process is responsible for the threshold behavior of the 2219 alloy.

References

[1] M.A. Moris, Phil. Mag. 65 (1992) 943.
[2] S. Kazanjian, N. Wang, E.A. Starke, Mater. Sci. Eng. A234-236 (1997) 571.
[3] J. Wang, X. Wu, K. Xia, Mater. Sci. Eng. A234–236 (1997) 287.
[4] P.K. Chaudhury, F.A. Mohamed, Metall. Trans. 18A (1987) 2105.
[5] P.K. Chaudhury, F.A. Mohamed, Mater. Sci. Eng. A101 (1988) 13.
[6] K.T. Park, E. Lavernia, F. Mohamed, Acta Metall. Mater. 42 (1994) 667.
[7] L. Kloc, S. Spigarelli, E. Cerri, E. Evangelista, T. Langdon, Acta Mater. 45 (1997) 529.
[8] Y. Li, T.G. Langdon, Acta Mater. 47 (1999) 3395.
[9] A. Brahma, T. Gerique, M. Torralba, M. Leiblich, Mater. Sci. Eng. A246 (1998) 55.
[10] P.B. Hirsh, A. Howie, R.B. Nicholson, D.W. Pashley, M.J. Whelan, Electron Microscopy of Thin Crystals, Butterworths, London, 1965, p. 574.
[11] J. Cadek, Creep in Metallic Materials, Academia, Praque, 1994, p. 304.
[12] O.A. Sherby, R.H. Klundt, A.L. Miller, Metall. Trans. 8A (1977) 843.
[13] O.D. Sherby, J. Wadsworth, Prog. Mater. Sci. 33 (1989) 166.
[14] M.R. Drury, F.J. Humphreys, Acta Metall. 34 (1986) 2259.
[15] R. Pickens, T.J. Langan, R.O. England, M. Liebson, Metall. Trans. 18A (1987) 303.
[16] H. Luthy, A. Miller, O. Sherby, Acta Metall. 28 (1980) 169.
[17] S. Raj, T. Langdon, Acta Metall. 37 (1989) 843.
[18] Landolt-Börnstein, Numerical data and functional relationships in science and technology, New Series. Group III: Crystals and solid state physics. Diffusion in solid metals and alloys, Berlin, 1990, pp.60, 628.
[19] Commercial aluminum alloys, Moscow, Metallurgy, 1984, 396.
[20] Y. Li, S.R. Nutt, F.A. Mohamed, Acta Mater. 45 (1997) 2607.
[21] E. Arzt, J. Rösler, Acta Metall. 36 (1988) 1053.
[22] J. Rosler, E. Arzt, Acta Metall. Mater. 38 (1990) 671.
[23] O.D. Sherby, P.M. Burke, Prog. Mater. Sci. 13 (1967) 325.
[24] A.K. Mukherjee, J.E. Bird, J.E. Dorn, Trans. Am. Soc. Metals 61 (1968) 696.
[25] D. Lesuer, C.K. Syn, J.D. Whittenberger, M. Carsi, O.A. Ruano, O.D. Sherby, Mater. Sci. Eng. 2001, accepted for publication.
[26] A.M. Jansen, D.C. Dunand, Acta Mater. 45 (1997) 4583.
[27] J. Cadek, S.J. Zhu, K. Milicka, Mater. Sci. Eng. A248 (1998) 65.
[28] J. Cadek, K. Kucharova, S.J. Zhu, Mater. Sci. Eng. A281 (2000) 162.
[29] D.C. Dunand, A.M. Jansen, Acta Mater. 45 (1997) 4569.
[30] J. Weertman, J. Appl. Phys. 28 (1957) 362.